Grant Agreement No: 101096307

Full Title: THz Industrial Mesh Networks in Smart Sensing and Propagation Environments

Start date: 01/01/2023

End date: 31/12/2025

Duration: 36 Months

Deliverable D5.2

THz Front-End Module Development

Document Type	Deliverable
Title	D5.2–THz Front-Ends Module Development
Contractual due date	--
Actual submission date	03/12/2025
Nature	Report
Dissemination Level	PUB
Lead Beneficiary	Fraunhofer IAF
Responsible Author	Sébastien Chartier (FRAUNHOFER)
Contributions from	Sandrine Wagner (FRAUNHOFER), Joscha Hoffmann (FRAUNHOFER)

Revision history

Version	Issue Date	Changes	Contributor(s)
V0.1	03/12/2025	Initial version	Sandrine Wagner (FRAUNHOFER), Joscha Hoffmann (FRAUNHOFER)
V0.2	11/12/2025	Review	- Contributors of V1.0 - Víctor Torres (ANTERAL)
V0.3	16/12/2025	Review	- Contributors of V1.1 - Varvara Elesina (TUBS)
V1.0	27/12/2025	Final Version	Luca Sanguinetti (CNIT), Thomas Kurner (TUBS)

Table of Contents

List of Abbreviations

- **CAD** – Computer Assisted Design
- **CNC** – Computer Numerical Control
- **EMI** – Electromagnetic Interference
- **IDU** – Indoor Unit
- **IF** – Intermediate Frequency
- **InGaAs** – Indium Gallium Arsenide
- **KPI** – Key Performance Indicator
- **LO** – Local Oscillator
- **mHEMT** – Metamorphic High Electron Mobility Transistor
- **MMIC** – Monolithic Microwave Integrated Circuit
- **MPA** – Medium Power Amplifier
- **P1dB** – 1 dB Compression Point
- **PA** – Power Amplifier
- **PCB** – Printed Circuit Board
- **PLL** – Phase-Locked Loop
- **RF** – Radio Frequency
- **Rx** – Receiver
- **SMT** – Surface Mount Technology
- **S-parameters** – Scattering Parameters
- **SPI** – Serial Peripheral Interface
- **TE10** – Transverse Electric mode
- **THz** – Terahertz
- **Tx** – Transmitter
- **UART** – Universal Asynchronous Receiver-Transmitter
- **USB** – Universal Serial Bus
- **VCO** – Voltage-Controlled Oscillator
- **VGA** – Variable Gain Amplifier
- **WR-3.4 / WR-12** – Waveguide sizes (WR = Waveguide Rectangular)
- **µC** – Microcontroller

Executive Summary

This report presents the final results of the TIMES THz front-end development activities. Building on front-end circuits designed and fabricated using Fraunhofer IAF's 35 nm InGaAs metamorphic high-electron-mobility transistor (mHEMT) technology, as documented in D5.1 [1], a fully integrated THz front ends has been completed. The platform comprises 300-GHz Rx and Tx waveguide modules, a high-performance Medium Power Amplifier (MPA), and PLL-based LO generation, delivering a coherent, end-to-end front-end solution.

The mechanical and RF architecture were executed to ensure low-loss, broadband operation in WR-3.4 and WR-12 modules. Key features include precision CNC-milled split-block housings, gold plating for enhanced conductivity and corrosion resistance, and E-plane probe transitions on an ultra-low loss fused silica dielectric for efficient MMIC-to-waveguide coupling. The integration approach—substantiated by detailed block diagrams and photographs—consolidates RF, PLL, and control electronics within a compact indoor unit (IDU) form factor, confirming manufacturability and system readiness.

Power amplifier developments are conclusive. The broadband designs achieve high gain over 270–315 GHz, while higher-power variants such as the AMP126MF300 demonstrate high saturated output at 300 GHz under optimal bias—meeting practical transmit power targets for THz links. Large-signal measurements confirm that output power scales with drain voltage, and small-signal S-parameters validate the intended flat-gain response, indicating design maturity and reproducibility.

Overall, the finalized results confirm that the TIMES THz front ends decisively meet excellent performance in gain, bandwidth, integration, and output power. The demonstrated 260–330 GHz coverage, conversion gain, integrated X8 LO chains, and high saturated MPA output establish a robust, manufacturable baseline and provide a convincing foundation for high-impact system-level demonstrations and subsequent deployment.

1. Introduction

1.1 Scope

This deliverable document reports on the final results of the THz front-end development. The general scope is the description of the fabricated front ends, including crucial design considerations, and to provide a summary of the final measurement results in comparison to the targeted specifications [2].

1.2 Audience

This report is intended for public use.

1.3 Structure

The core of the document is structured as follows:

- Section 2 provides a detailed overview of the different components (Tx, Rx, MPA, PLL, …) of the indoor unit
- Section 3 presents the characterization results of the aforementioned components as well as analysis and assessment of the performance
- Finally, section 4 presents the results of the Indoor Unit measurement campaign.

2 Front-End Development

2.1 Functional Block Diagram

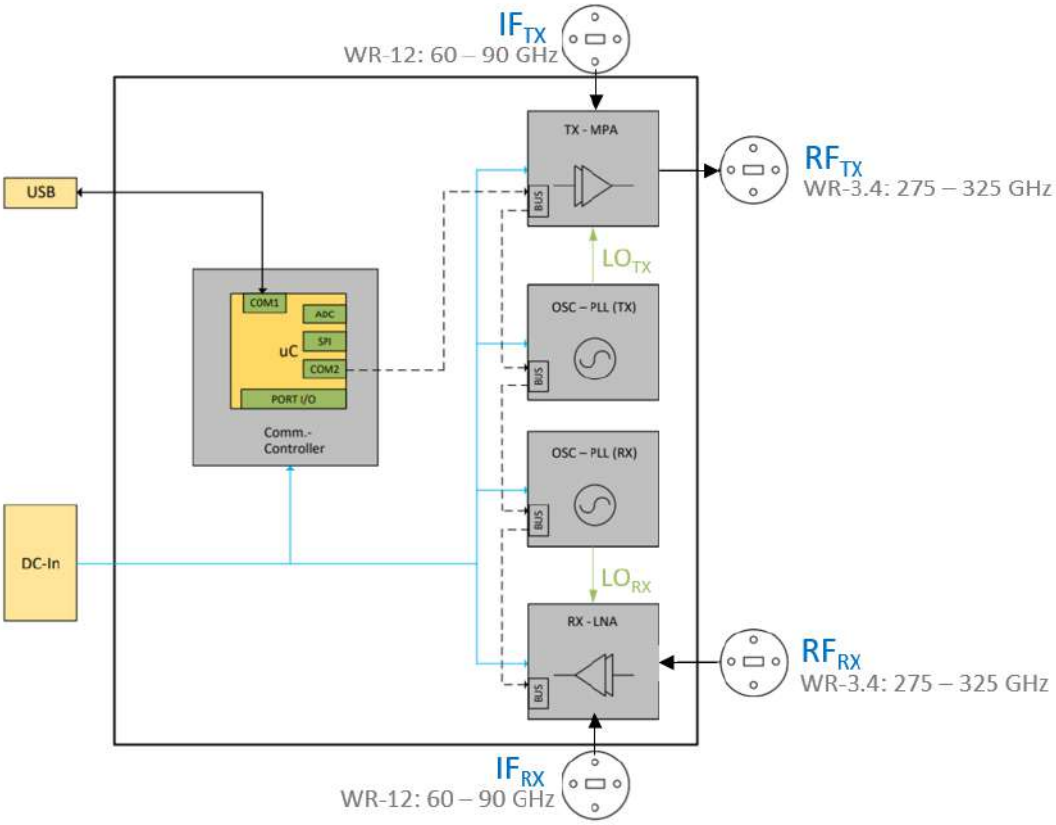

Figure 1: Block diagram of the THz front ends including Tx and Rx waveguide modules as well as the PLLs for the LO signal generation and Comm.-Controller for the bias and frequency control.

Figure 1 presents the functional block diagram of the TIMES Indoor Units (IDUs), depicting an integrated heterodyne transceiver front end operating over 275–325 GHz with IF interfaces in the 60–90 GHz range. RF input and output are implemented via WR-3.4 waveguide ports, while IF interfaces employ WR-12. The architecture supports full-duplex operation with distinct transmit and receive paths.

In the transmit chain, a 60–90 GHz signal applied at the IF_{Tx} port is routed to the medium power amplifier (MPA) block, which performs up-conversion and, optionally, medium-power amplification. Up-conversion is realized by mixing the IF signal with a local oscillator tone, LO_{Tx}, provided by a dedicated oscillator–PLL unit. The resulting 275–325 GHz RF output is delivered at the RF_{Tx} port.

On the receive side, an RF signal entering at the RF_{Rx} port is initially amplified by a low-noise amplifier to ensure a low system noise figure. The amplified signal is subsequently down-converted on the same receiver MMIC using LO_{Rx}, generated by a second oscillator–PLL unit. The resulting IF signal in the 60–90 GHz band is presented at the $IF_{sub\text{-}th}$ port.

The local oscillators employ PLL synthesizers with integrated VCOs and are digitally configured via a common SPI interface. These PLLs provide the frequency agility and phase stability required for high–data-rate communications and beam steering.

System control is implemented by an embedded communication controller based on a microcontroller (µC). The controller is responsible for SPI communication, monitoring, and peripheral I/O through a unified firmware interface. USB connectivity enables computer interaction, while the DC-In block powers the unit. The controller manages initialization, bias sequencing, telemetry acquisition, and digital interfacing with the PLLs and Tx/Rx chains.

The architecture supports modularity and closed-loop control, enabling automated tuning and parameter monitoring as well as straightforward upgrades. Digital bus routing and signal distribution are optimized for compact integration and low cross-talk. The frequency plan, component partitioning, and control logic collectively render the system suitable for both laboratory and field deployments at THz frequencies.

2.2 Front-End Implementation

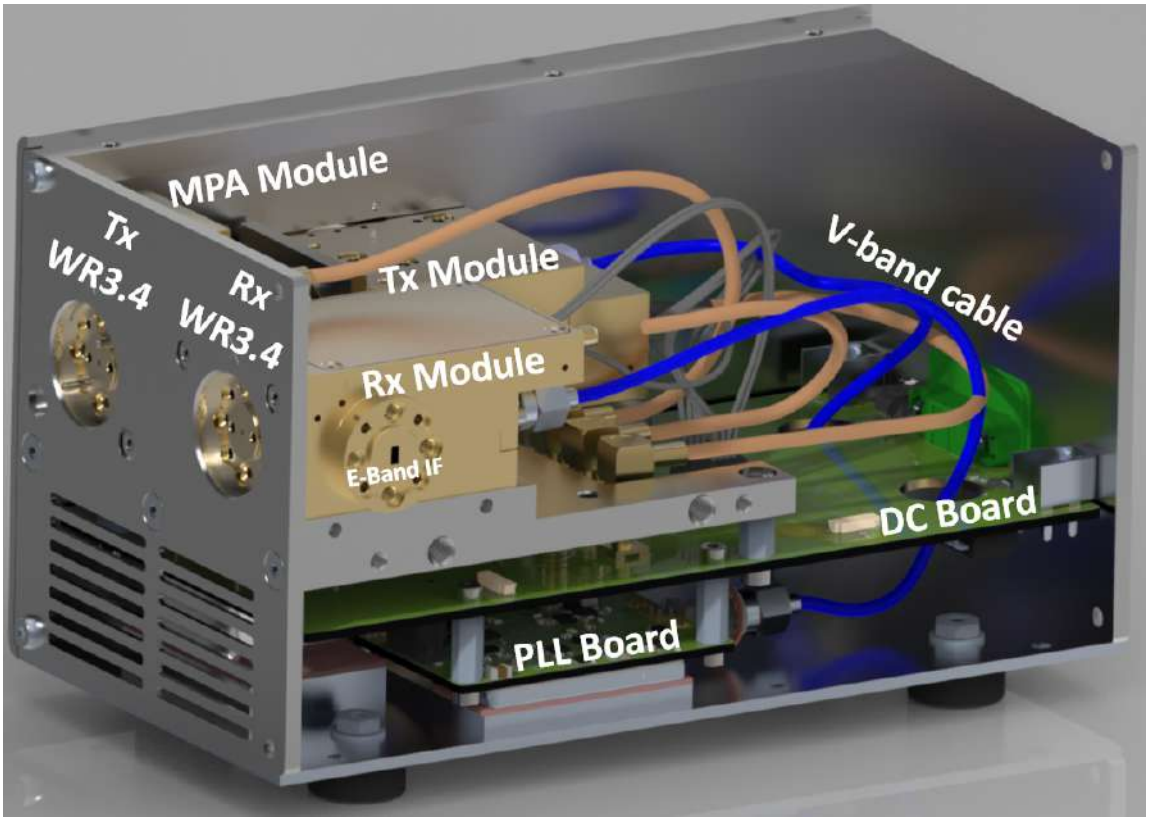

Figure 2: Illustration of the open Indoor Unit, including the Rx, Tx and MPA waveguide housings, the PLL for signal generation and the WR-3.4 waveguide interface The IDU has a dimension of 17.2x8.9x7.2 cm³.

Figure 2 presents a CAD view of the THz Indoor Unit (IDU), highlighting the internal arrangement of key RF and electronic subsystems. The modules are integrated within a metallic enclosure that provides front-panel access to the WR-3.4 waveguide flanges for the transmit and receive paths, with WR-12 IF waveguide

interfaces located on the side. Both Tx and Rx ports are specified as WR-3.4, supporting operation across 275–325 GHz.

Within the enclosure, the RF chain is implemented using modular blocks mounted on a layered mechanical stack incorporating the DC and PLL boards. The receive module is placed nearest to the front panel and directly interfaces with the WR-3.4 Rx flange, providing down-conversion of THz signals to an E-band IF (60–90 GHz). Adjacent to it, the transmit module performs up-conversion of the E-band IF to the WR-3.4 output band. The upconverted signal is routed via a short waveguide to the mounted MPA, which secures sufficient output level and preserves spectral purity at the final RF port. The minimized waveguide run reduces path loss and enhances mechanical robustness.

Interconnects between the RF modules and the underlying PLL boards are realized using flexible V-band coaxial cables, dimensioned and routed to respect bending-radius constraints. Beneath the RF plane, electronics are distributed across two stacked printed-circuit boards. The upper DC board implements power conditioning and voltage regulation for the RF and control subsystems, including sequencing, bias generation, and telemetry acquisition. The lower PLL board generates the local oscillator tones for up- and down-conversion and hosts digitally controlled oscillator–PLL units interfaced to the microcontroller. Thermal management and RF shielding are addressed through vertical stacking and mechanical segregation of noisy digital sections from sensitive RF paths.

The metal housing (see Figure 3) incorporates WR-3.4 interfaces compatible with the anticipated antenna and splitter configurations. Its modularity enables data-link evaluation with or without the MPA, facilitating testing and rapid reconfiguration. Overall, the layout evidences a compact, modular design optimized for low-loss RF routing, effective heat dissipation, and mechanical stability in a transceiver, suitable for laboratory validation, prototyping, and integration into advanced communication systems.

Figure 3: Photograph of the Indoor Unit casing

2.3 PLL Development

The PLL subsystem is specified to generate an adjustable local oscillator (LO) signal over 24–33.6 GHz with an output power of approximately 3–7 dBm. The LO frequency is incrementable and decrementable with a defined step size to support deterministic tuning. The RF signal chain of the PLL is presented in Figure 4.

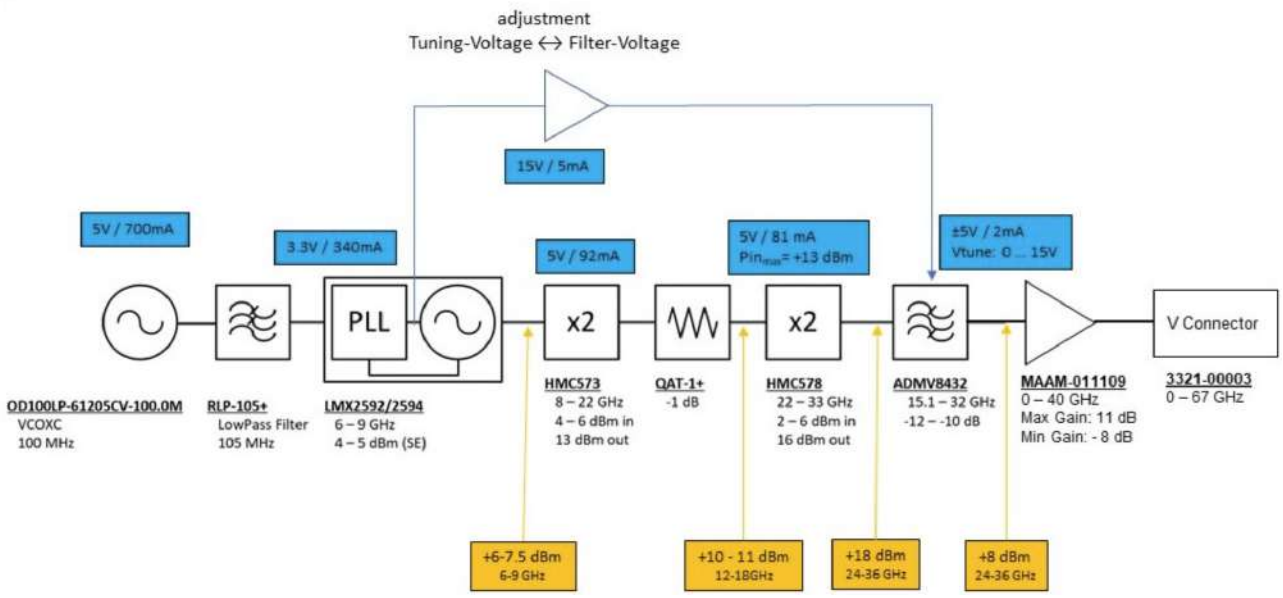

Figure 4: RF signal chain of the PLL

As no monolithic PLL ICs natively cover 24–33.6 GHz, the architecture employs the Texas Instruments LMX2595 to synthesize a 6–8.4 GHz signal, which is subsequently frequency-quadrupled to 24–33.6 GHz using two cascaded multiplier stages. Unwanted harmonics are suppressed by the tunable bandpass filter ADMV8432, ensuring spectral cleanliness across the tuning range. Output power is set by the MAAM-011109 VGA, enabling precise level control within the 3–7 dBm target.
The LO connector is a 1.85 mm edge-launch connector, providing a coaxial interface to the Rx/Tx modules and supporting low-loss, high-frequency signal delivery. Frequency stepping, amplitude control, and filter tuning are integrated into the digital control scheme to ensure agile, repeatable LO synthesis across the specified band. Figure 5 presents the layer structure of the PCB used for the PLL.

Board Layer Stack	Layer	Material	Thickness	Dielectric constant
	1	Copper	35 µm	
		RO4350B	168 µm	3.48
	2	Copper	18 µm	
		FR-4	1 mm	4.3
	3	Copper	18 µm	
		RO4350B	168 µm	3.48
	4	Copper	35 µm	

Figure 5: Layer structure of the PLL PCB (each colour within the left column corresponds to a specific material)

The RF signal chain of the PLL is located on Layer 1. Layer 2 is a GND plane for shielding the RF signal. The RF signal chain is shielded against interference by an EMI shield. The Top side layout of the PLL PCB is presented in Figure 6.

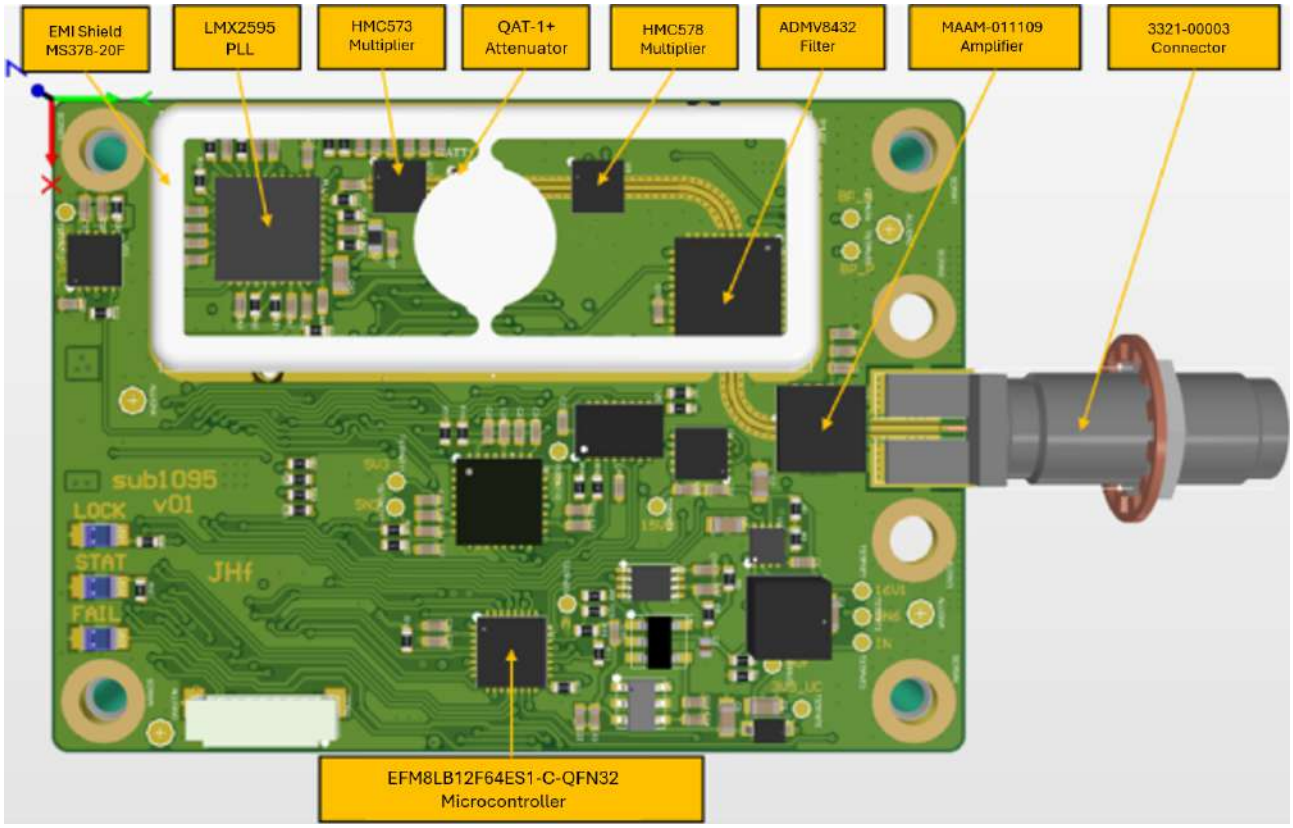

Figure 6: Top side layout of the PLL PCB

A block diagram of the overall PLL PCB with the reference oscillator PCB (PCB REFOSC) and the two attached PLL PCBs 1 and 2 is presented in Figure 7.

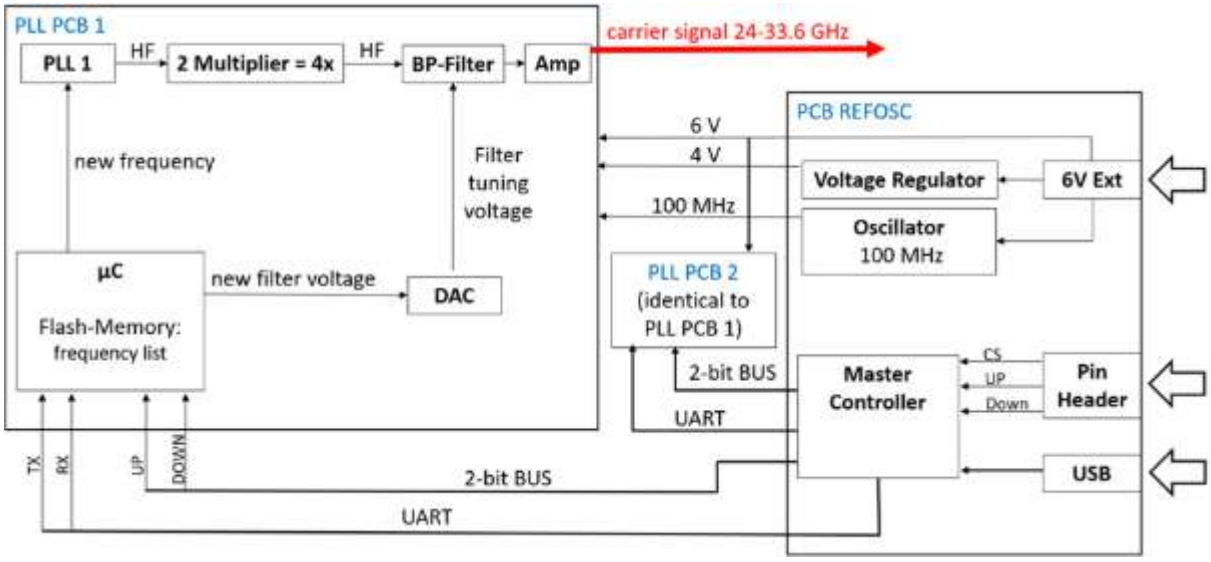

Figure 7: Block diagram of the PLL PCBs 1 and 2 together with the reference oscillator PCB (PCB REFOSC) and the two attached PLL PCBs

The REFOSC PCB supplies regulated voltages to both PLLs and the Rx/Tx modules and distributes a common frequency reference. A 100 MHz reference is generated by a voltage-controlled crystal oscillator (VCXO), OD100LP-61205CV-100M (Connor-Winfield). Reference harmonics are suppressed by the RLP-105+ low-pass filter, and the filtered signal is apportioned to both PLLs via a resistive power divider. A master microcontroller on the REFOSC PCB manages the two PLLs over a UART interface.
To enable rapid, incremental PLL retuning, the REFOSC PCB provides a pin-header hardware interface. Any PLL can be stepped through a predefined frequency list using active-low Up/Down lines; device targeting is performed via a Chip Select line (Low selects PLL1, High selects PLL2). PLL1 is assigned to the Tx path and PLL2 to the Rx path.
All PLL register configurations and adjustable voltage setpoints for the PLL board are stored in the microcontroller's flash memory. During frequency stepping via the Up/Down inputs, time-intensive flash writes are bypassed; consequently, after a power cycle, each PLL reverts to the last frequency configured over USB. The Photograph of top- and backside of the assembled PLL board is shown in Figure 8.

The following table lists the frequencies accessible via the Up/Down interface.

Predefined frequency list in GHz					
24	25.6	27.2	28.8	30.4	33.6
24.4	26	27.6	29.2	31.2	
24.8	26.4	28	29.6	32	
25.2	26.8	28.4	30	32.8	

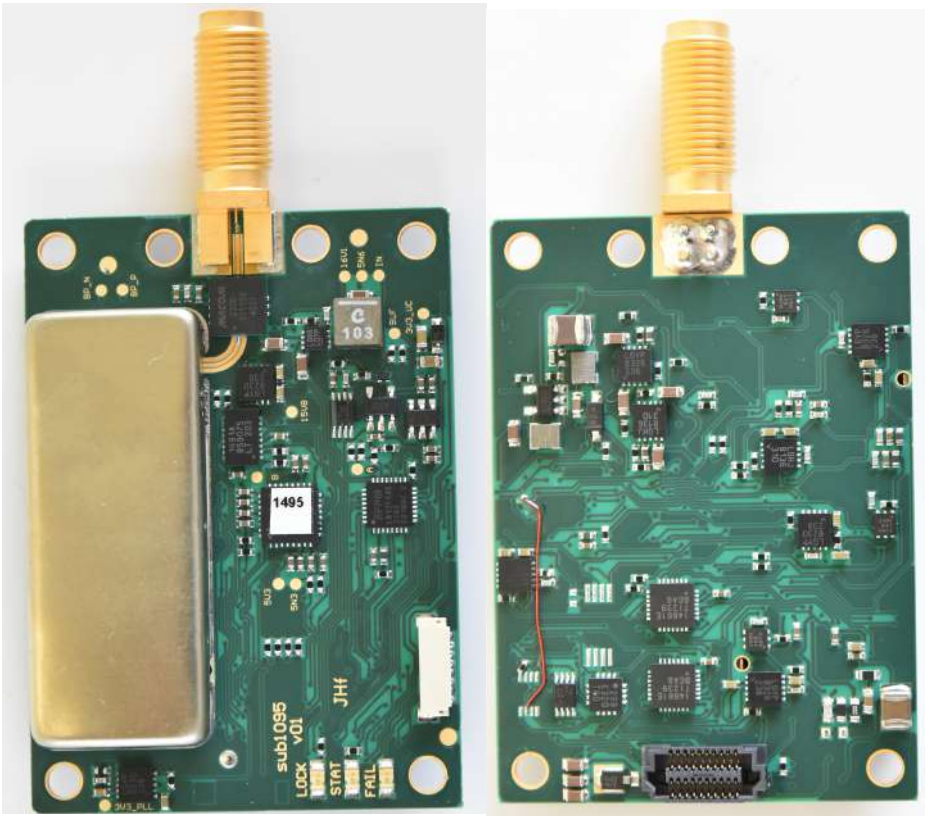

Figure 8: Photograph of top- and backside of the assembled PLL board

2.4 Tx-Module Implementation

Fraunhofer IAF assembles the TIMES THz MMICs [1] in CNC-milled, gold-plated split-block rectangular-waveguide modules to suppress surface oxidation, minimize conductor loss, provide a stable RF ground, and ensure an efficient thermal path. The two housing halves define the waveguide channels, probe cavities, and λ/4 backshort recesses; the lower half carries the MMIC and any transition substrates, while the upper half completes the electromagnetic boundary conditions and sets the backshort spacing. External interfaces use band-matched standard flanges (WR-12 for IF and WR-3/WR-3.4 for 300 GHz RF in the 300-GHz front ends). Tight tolerances on waveguide width/height and backshort distance mitigate TE10 detuning and suppress higher-order mode conversion across the operating bands.

Two complementary planar-to-waveguide coupling strategies are employed. For multi-port front ends that route LO, RF, and IF in distinct bands, micromachined fused-silica E-plane probe transitions are used. A 50 µm fused-silica tile carries a microstrip that extends as an E-plane probe into the waveguide; a quarter-guided-wavelength backshort furnishes the primary match. The microstrip interfaces to MMIC pads via short, parallel gold wedge bonds to minimize series inductance and radiation. In the 300-GHz transmitter/receiver modules, the WR-12 IF transitions exhibit < 1 dB insertion loss and > 15 dB return loss from 57 to > 90 GHz, while the RF transition loss at 300 GHz is typically 1–2 dB. For compact single-path amplifier modules, the E-plane probe is integrated directly on the MMIC substrate (typically 50 µm GaAs), eliminating RF bond wires in the main path. This approach has demonstrated < 0.5 dB transition loss around 250 GHz and enables low module loss with the MMIC embedded in a WR-3 split block.

Die placement is registered to a machined pedestal that defines the electrical reference plane and limits cavity height above the circuit. Where fused-silica probe tiles are used, the probe is located in the waveguide E-plane and the upper block provides the conducting backshort; final spacing is established via co-simulation and validated on the assembled hardware. RF interconnects use short, parallel 25 µm gold wedge bonds with controlled length to realize extremely low inductance. Bias and control lines are routed with RF chokes and via fences to suppress slot-mode excitation at the split plane. Gold plating of the brass blocks reduces surface resistance and improves flange-to-flange repeatability, while the block mass furnishes an effective thermal path from the MMIC through the pedestal to the module body.

Front-end modules integrate on-board bias generation and current sensing to reduce harness complexity and enhance stability. A single positive supply in the 3.3–5 V range feeds local regulation and monitoring. RF interfaces are WR-3 at 300 GHz and WR-12 for IF. In the same technology node, packaged MPA modules employ integrated MMIC-to-waveguide transitions on 50 µm GaAs rather than fused-silica tiles, thereby eliminating RF bond wires and further reducing transition loss; these MPAs are delivered as a dedicated module series, distinct from the front-end assemblies.

The assembly flow proceeds as follows: co-design of electromagnetic and mechanical features (waveguide channels, probe cavities, backshort recesses), CNC milling, cleaning, and gold plating of housings, fabrication and RF verification of fused-silica probe tiles (when applicable), die attach of MMICs on the pedestal for optimal thermal/RF contact; placement and bonding of probe tiles to the MMIC with short RF wires, completion of bias-network interconnects, alignment and fastening of the upper block to set the backshort and close waveguide paths. Modules with integrated on-chip probes omit the fused-silica tile and main-path RF bonds. Following electrical checkout of the integrated bias board, waveguide-level characterization is performed with band-appropriate extenders, including S-parameters, conversion gain, compression, and noise where applicable, and verification of IF routing and isolation per use case.

This packaging strategy is driven by the RF budget, where transition loss, bond parasitics, and waveguide leakage dominate. Confining fields to well-defined metal waveguides, employing E-plane probes with quarter-wave backshorts, and integrating the probe on chip wherever feasible minimizes discontinuities, resistive losses, and radiation. Gold-plated split blocks provide stable grounds and robust thermal anchoring. The resulting modules closely track on-wafer MMIC performance and deliver reproducible, broadband coupling suitable for high-performance communication demonstrators.

A simplified block diagram as well as a photograph of the Tx-Module front-end are shown in Figure 9 and Figure 10, respectively. A detailed photograph of the inner part of the Tx module is presented in Figure 11. The front-end module is based on two MMICs: a by-four frequency multiplier MMIC (see Figure 12 that is used to feed the LO-port of a THz up-converter chain MMIC (see Figure 13). The module assembly follows the aforementioned approach.

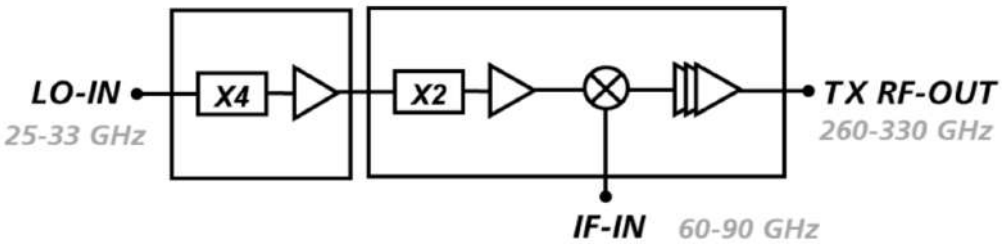

Figure 9: Simplified block diagram of the Tx-Module front-end

Figure 10: Photograph of the Tx waveguide module

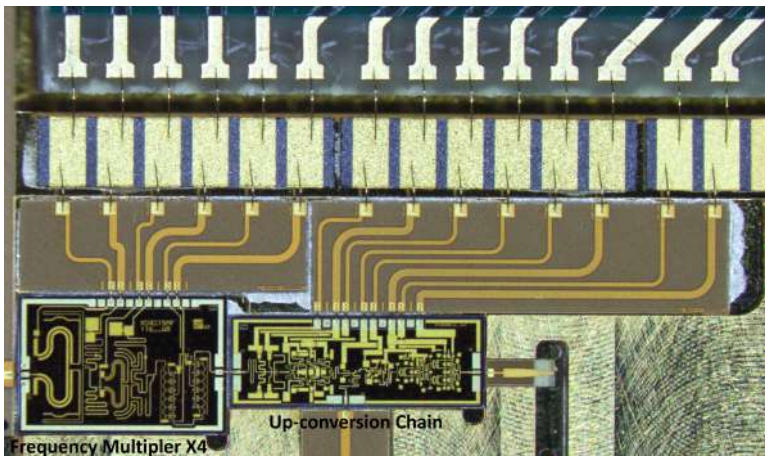

Figure 11: Detailed photograph of the inner part of the Tx module.

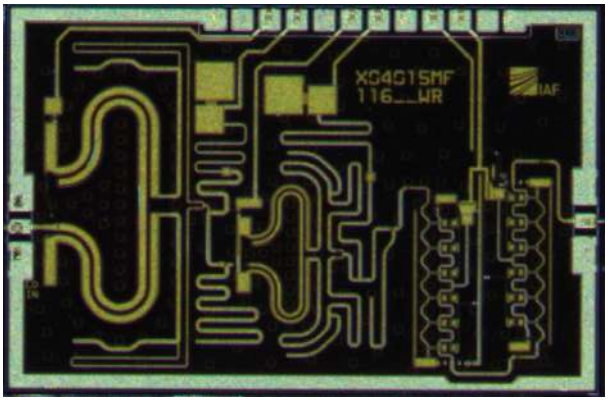

Figure 12: Detailed photograph of the by-four-frequency multiplier

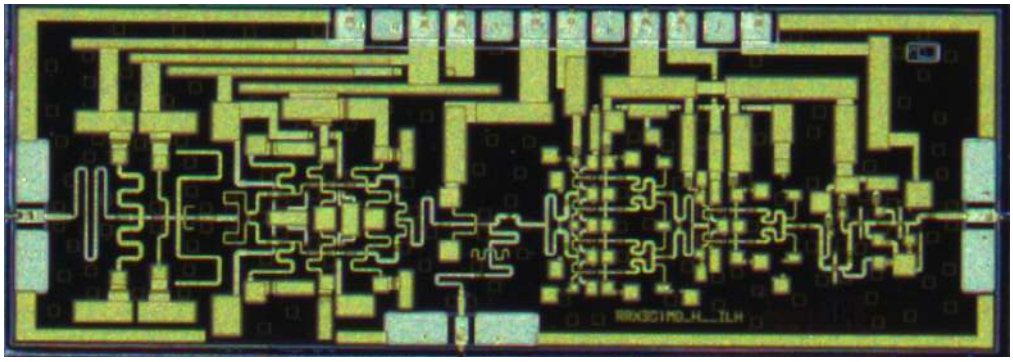

Figure 13: Detailed photograph of the Tx front-end MMIC.

2.5 Rx-Module Implementation

The assembly of the Rx waveguide module follows the identical approach described in the Tx-Module Implementation chapter. The simplified block diagram of the Rx front-end is presented in Figure 14 and a Photograph of the waveguide module is presented in Figure 15. A detailed photograph of the module is showed in Figure 16.

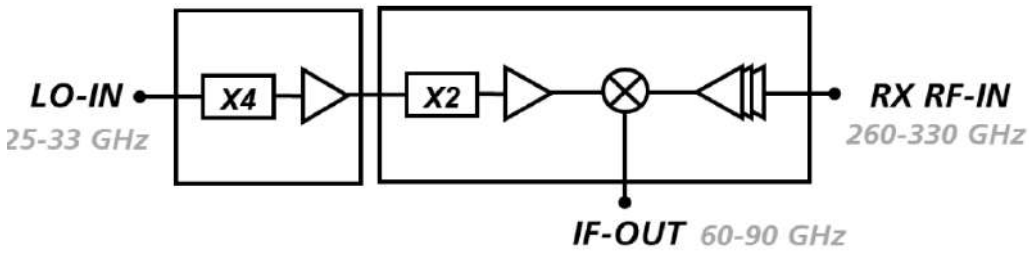

Figure 14: Simplified block diagram of the Rx module architecture.

Figure 15: Detailed photograph of the Rx front-end module.

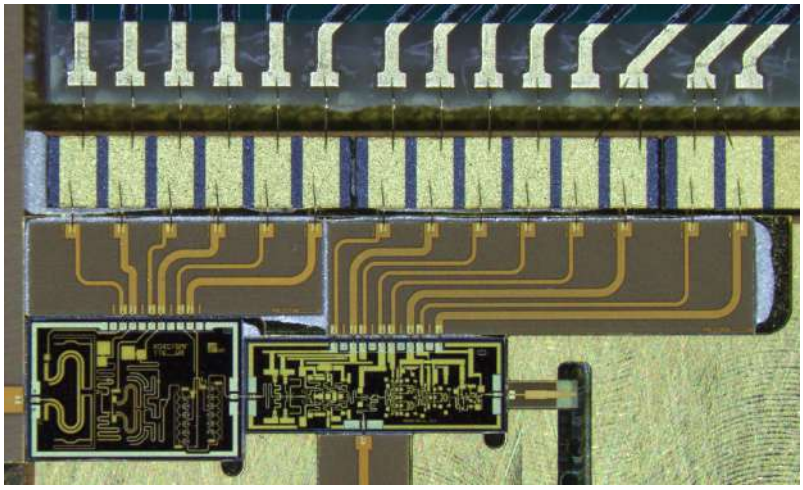

Figure 16: Detailed photograph of the Rx module.

2.6 Medium Power Amplifier Implementation

This chapter details the design of the compact 260–320 GHz power amplifier (MPA) delivering >10 mW output power. Implemented in IAF's 35-nm InGaAs mHEMT technology, the MPA employs a six-stage architecture that minimizes die area while maximizing gain and power density. A central innovation is the complete decoupling of DC bias and RF matching through dedicated vertical interconnects, enabling high transistor density with independent impedance control.

Conventional THz PAs face biasing constraints when parallelizing devices, often embedding DC distribution within RF paths or relying on vertical bias lines that compromise RF matching and stability. The presented topology segregates the vertical gate and drain bias networks from the RF circuitry, thereby improving matching flexibility, reducing parasitic coupling, and simplifying bias management.

Each gain stage comprises four common-source transistors arranged in a compact power-bar layout. Transistor finger widths increase from 10 µm at the input to 16 µm at the output, for a total effective width of 512 µm per stage. The vertical biasing scheme shortens bias return paths and mitigates RF interference and oscillation risk, supporting stable broadband operation across 260–320 GHz.

The MPA MMIC overall performance was assessed with standard RF pads (see Figure 17), while the MPA MMIC to be assembled contains, as previously mentioned, e-plane probes to significantly simplifies the assembly process.

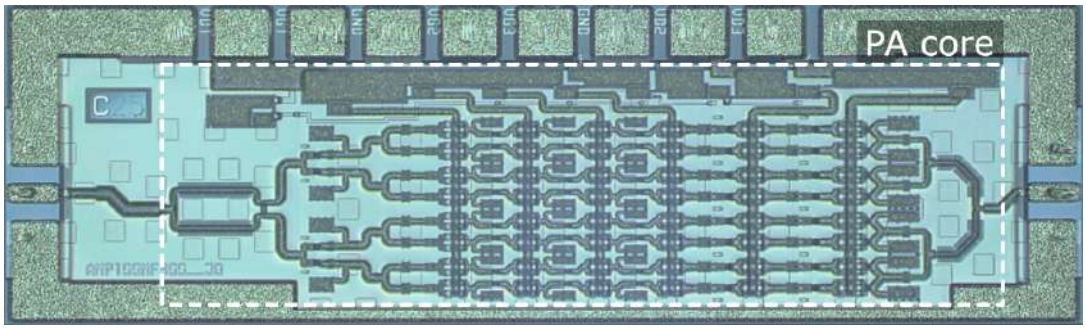

Figure 17: Chip photographs of the developed 300-GHz power amplifier MMIC (without e-plane probe interface).

2.7 Planar THz assembly

In addition to the previously presented waveguide modules, a compact, low-cost THz frequency-conversion module was designed by consolidating all RF, analogue, digital control, and thermal functions into a thin, two-plate housing with minimal part count and direct waveguide interfaces. Frequency conversion between a WR-3.4 RF port (220–325 GHz) and a WR-12 high-IF port (56–90 GHz) was designed in a single gold-plated block mounted on a low-loss PCB, eliminating bulky interconnects and reducing the mechanical envelope to a hand-sized footprint.

Compactness was achieved through a stacked architecture in which the machined RF block sits directly on the PCB and couples to the front WR-3.4 flange with a short, uninterrupted transition. The WR-12 IF flange exits near the top edge of the assembly, maintaining a rigid, short path while avoiding mechanical interference with the RF aperture. The enclosure consists of metal plates that serve simultaneously as structural faces, RF shields, and heat spreaders.

The low-cost potential derives from the deliberate reduction of unique parts and the use of standard, readily available components and processes. The RF core is a single gold-plated cavity block rather than a multi-piece

stack, lowering machining time, tolerances, and alignment effort. The housing plates are simple planar geometries suitable for standard CNC fabrication in batch processes. Both waveguide ports follow standard WR-3.4 and WR-12 flange conventions, enabling procurement of mating horns, lenses, and fixtures off the shelf and avoiding custom connectors. The PCB integrates power entry, bias control, and digital configuration with commercial components, allowing the RF block to be built and tested with turnkey SMT assembly and minimal post-fabrication tuning.

Thermal stabilization is provided without the use of expensive thermoelectric cooler or large heat sinks. The RF block is clamped to the plates for efficient conduction, while a small side bracket carries two miniature axial fans that sweep airflow across the PCB hotspots and the RF block surface. This arrangement maintains temperature stability with low power and negligible volume penalty, and the bracket can be manufactured as a single, low-complexity part. By isolating the fans from the RF block, vibration transmission to the waveguide joints is minimized without adding damping components. The use of the axial fans is based on the experienced acquired during the development of the waveguide modules previously presented where temperature rose to an uncritical but noticeable range.

Additionally, it is important to mention that the direct waveguide-to-waveguide approach avoids expensive high-frequency coaxial lines and precision adapters, improves yield through repeatable flange alignment, and shortens test cycles. The Concept for the planar THz assembly is presented in Figure 18.

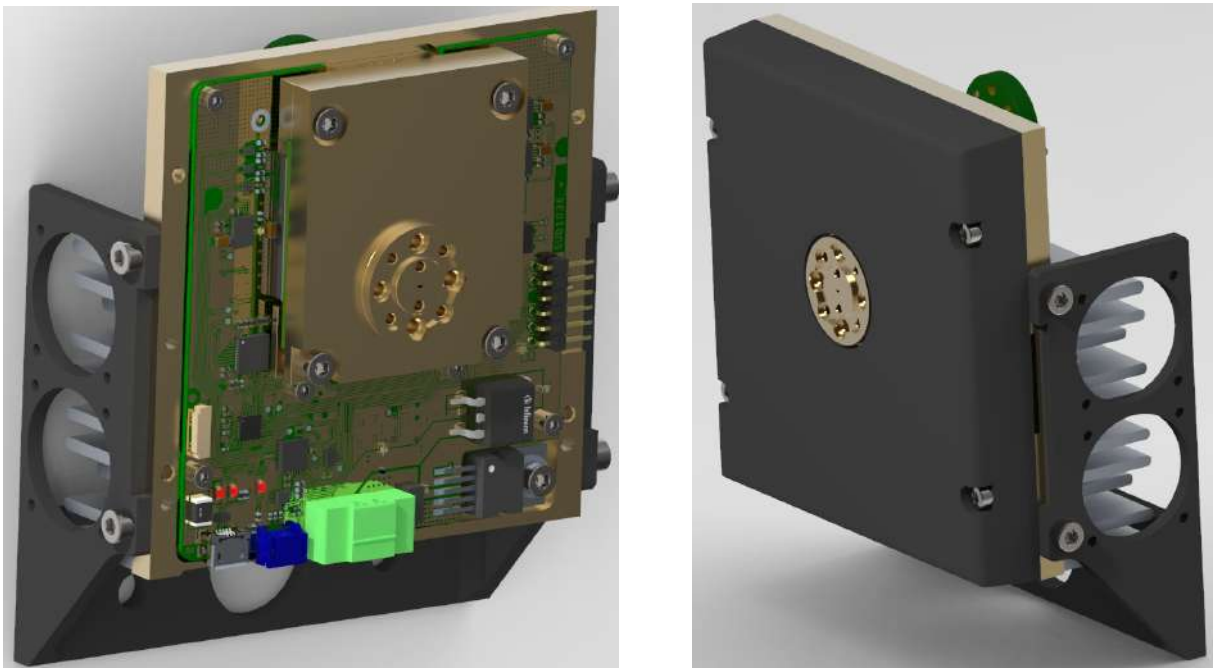

Figure 18: Concept for the planar THz assembly

Additionally, an H-Band transition was designed to efficiently couple between a rectangular waveguide and a 50-Ω microstrip transmission line fabricated on an ultra-low loss substrate. This interface is critical for

embedding the mHEMT THz circuits into waveguide modules. The transition concept employs an E-field probe that transforms the dominant waveguide mode into a quasi-TEM microstrip mode.

A fully parametric 3D electromagnetic test bench of the transition has been developed for the spectral range from 220 to 330 GHz using an electromagnetic field solver. The model accounts for the thin 50 µm substrate, which is used to limit dielectric losses while maintaining mechanical integrity. Gold metallization is assumed for the conductive regions, and a surface roughness of 300 nm is incorporated into the simulation framework to capture conductor-loss contributions with realistic accuracy at THz frequencies.

To experimentally validate the transition, a dedicated waveguide test module was designed in which the transition is realized in a back-to-back topology. In this configuration, electromagnetic energy is coupled from the waveguide to the microstrip line and then reconverted to the waveguide domain via a second, identical transition. Fabricating the structure enables direct measurement of the combined insertion loss of both transitions, including the short microstrip segment between them. Because the waveguide section introduces known attenuation, this approach allows the intrinsic performance of a single transition to be isolated by comparison with simulation.

Electromagnetic simulations predict an insertion loss of approximately 0.4 dB for an individual transition at frequencies near 300 GHz. Measurements of the back-to-back realization yield a total insertion loss of about 1.3 dB in the same frequency region. A significant fraction of this measured loss arises from the non-negligible attenuation within the waveguide itself, exacerbated by practical metallization roughness. The close correspondence between simulated and measured S-parameters confirms that the electromagnetic model accurately captures the behavior of the transition, including dielectric losses, conductor losses, and waveguide attenuation.

The agreement between simulation and experimental results validates the performance of the transition and confirms its suitability for high-frequency integration in H-Band waveguide modules. The low insertion loss and predictable behavior make it a robust interface for characterizing and operating MMIC circuits within THz waveguide systems. A detailed view of the dedicated back-to-back waveguide test module and simulation as well as measurement results are presented in Figure 19.

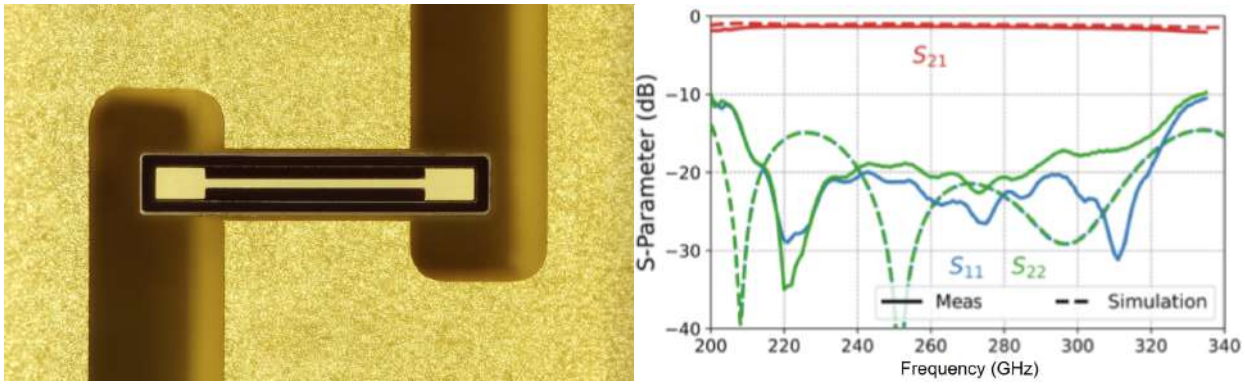

Figure 19: Detailed view of the dedicated back-to-back waveguide test module(left) and simulation as well as measurement results (right).

Identically, the E-Band transition was designed and simulated using HFSS. The simulation shows excellent performance such as low loss as well as very good matching over the entire E-Band. The used HFSS Testbench of the E-Band transition and simulation results are shown in Figure 20.

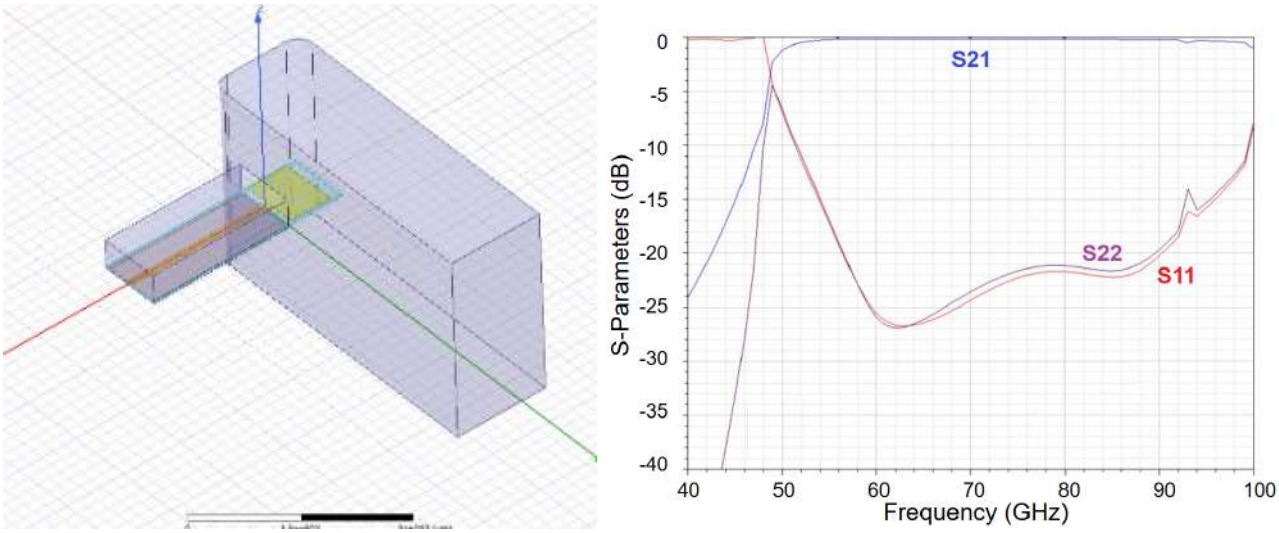

Figure 20: HFSS Testbench of the E-Band transition (Left) and simulation results (Right)

Over the course of the project, the complete THz/RF, mechanical, and PCB-level designs for the planar module were developed to a level of maturity that goes significantly beyond an early-phase design study. A complete PCB design was finalized, including RF, biasing, and digital-control routing. In parallel, detailed 3D electromagnetic simulations were performed for all critical transitions, including the WR-3.4 to microstrip coupling, the IF routing, and the internal interconnects. These simulations produced consistent results, confirming that the targeted RF performance—conversion gain, bandwidth, and transition loss—can be achieved using the proposed planar approach. Complementing this work, a complete mechanical CAD model of the module was generated, defining the stacked architecture, waveguide alignment features, thermal interfaces, and manufacturable geometries suitable for standard CNC processes.

Taken together, these elements constitute a technically validated blueprint for a fully manufacturable device. The close agreement between the EM results and the expected module-level performance strongly indicates that the final hardware can be realized without requiring major redesign steps. Furthermore, the mechanical design was reviewed with the highly experienced team of the Fraunhofer workshop and confirms compatibility with standard machining tolerances and assembly practices, thereby reinforcing the manufacturability of the concept.

While the assembly of the complete planar module could not yet be fully finalized, the achieved design, simulation, and CAD results significantly de-risk future fabrication. The work performed provides a clear, validated pathway to hardware realization and offers a solid basis for follow-up prototyping activities.

3 Front-End Characterization

3.1 Tx-Module Characterization

Table 1: Summary of the Tx-module performance.

Port	Parameter	Min	Typ	Max
DC	DC voltage @ connector	3.5 V	3.8 V	5 V
	DC current		245 mA	275 mA @ P-LO 2 dBm
	DC connector	SMB		
LO-IN	LO-IN input power	-4 dBm	2 dBm	4 dBm
	LO-IN input frequency	25 GHz		30 GHz
	LO-IN connector	V-Connector		
RF-OUT	RF-OUT output power		-5 dBm	0 dBm
	RF-OUT frequency range	270 GHz		330 GHz
	RF-OUT connector	H-Band waveguide (WR-3)		
IF	IF input power		-10 dBm	0 dBm
	IF frequency	60 GHz		90 GHz
	IF connector	E-Band waveguide (WR-12)		

*) all values referred to module interface

The transmitter module "M371RTXH" developed and manufactured in the frame of the TIMES project, using the aforementioned assembly approach, was characterized in a calibrated waveguide environment. A summary of the Tx-module performance is presented in Table 1. The measurements of the module are shown in Figure 21.

In the plot "RF output power vs LO power", the RF output power increases from approximately −40 dBm to about −5 dBm as the LO drive level is raised from roughly −12 dBm to 0 dBm, depending on the selected LO frequency band. For LO frequencies around 200 GHz, saturation of the RF output is observed already at LO power levels near −4 dBm to −2 dBm, while at higher LO frequencies around 240 GHz a higher LO drive is required to reach similar RF output levels. Beyond about 0 dBm LO power, the RF output power shows only marginal improvement, indicating clear saturation of the frequency conversion process.

The plot "RF output power vs IF Frequency" shows the RF output power as a function of IF frequency in the range from about 60 GHz to 90 GHz at a fixed IF input power of −10 dBm. Over a central IF frequency of roughly 80 GHz, the RF output power remains relatively flat. Outside this central IF frequency, a gradual roll-off of several dBs is observed, indicating IF bandwidth limitations and reduced conversion efficiency at the band edges.

The RF output power is plotted in "RF output power vs RF Frequency for diff LO Freq." versus RF frequency from about 260 GHz up to 330 GHz for different LO frequency ranges. For LO settings around 200–220 GHz, the RF output power reaches peak values close to 0 dBm in the RF band between approximately 285 GHz and 300 GHz. As the RF frequency increases beyond 310 GHz, the output power decreases by roughly 5–10 dB, depending on the LO frequency. Lower RF frequencies below about 270 GHz also show reduced output levels, confirming a usable RF bandwidth on the order of 30–50 GHz around the center frequency.

The dependence on LO tuning is highlighted in the plot "RF output power vs LO Frequency", where the LO frequency is swept from roughly 23 GHz to 33 GHz for several IF frequencies (70 GHz, 80 GHz, and 90 GHz) at a fixed LO input power of 2 dBm. The RF output power rises sharply from below −30 dBm to near 0 dBm

as the LO frequency enters the optimal range around 26–27 GHz. Maximum output power levels of approximately 0 dBm are observed between about 27 GHz and 29 GHz LO frequency. Outside this range, particularly above 30 GHz LO frequency, the RF output power drops again by more than 10 dB, demonstrating a well-defined optimal LO operating window.

The plot “RF output power vs RF Frequency for diff IF Freq.” presents the RF output power between approximately 260 GHz and 330 GHz for IF frequencies of 70 GHz, 80 GHz, and 90 GHz at a constant LO power of 2 dBm. For all IF settings, peak RF output levels close to 0 dBm are achieved in the central RF band around 290–305 GHz. At lower RF frequencies below about 270 GHz and higher RF frequencies above 320 GHz, the output power decreases significantly, in some cases below −10 dBm. The similarity of the curves indicates that changing the IF frequency mainly shifts the RF band position while preserving comparable peak output power levels.

Finally, “RF output power and compression vs IF input power” characterizes the large-signal behavior of the transmitter at an IF frequency of 80 GHz. As the IF input power increases, the RF output power increases nearly linearly, corresponding to a conversion gain on the order of 6–11 dB. For IF input powers above roughly −8 dBm, gain compression becomes apparent, and the RF output power approaches saturation near 0 dBm. The corresponding conversion gain curves show a clear reduction of several dBs in this regime, allowing the identification of the 1 dB compression region and confirming the usable linear input power range of the transmitter.

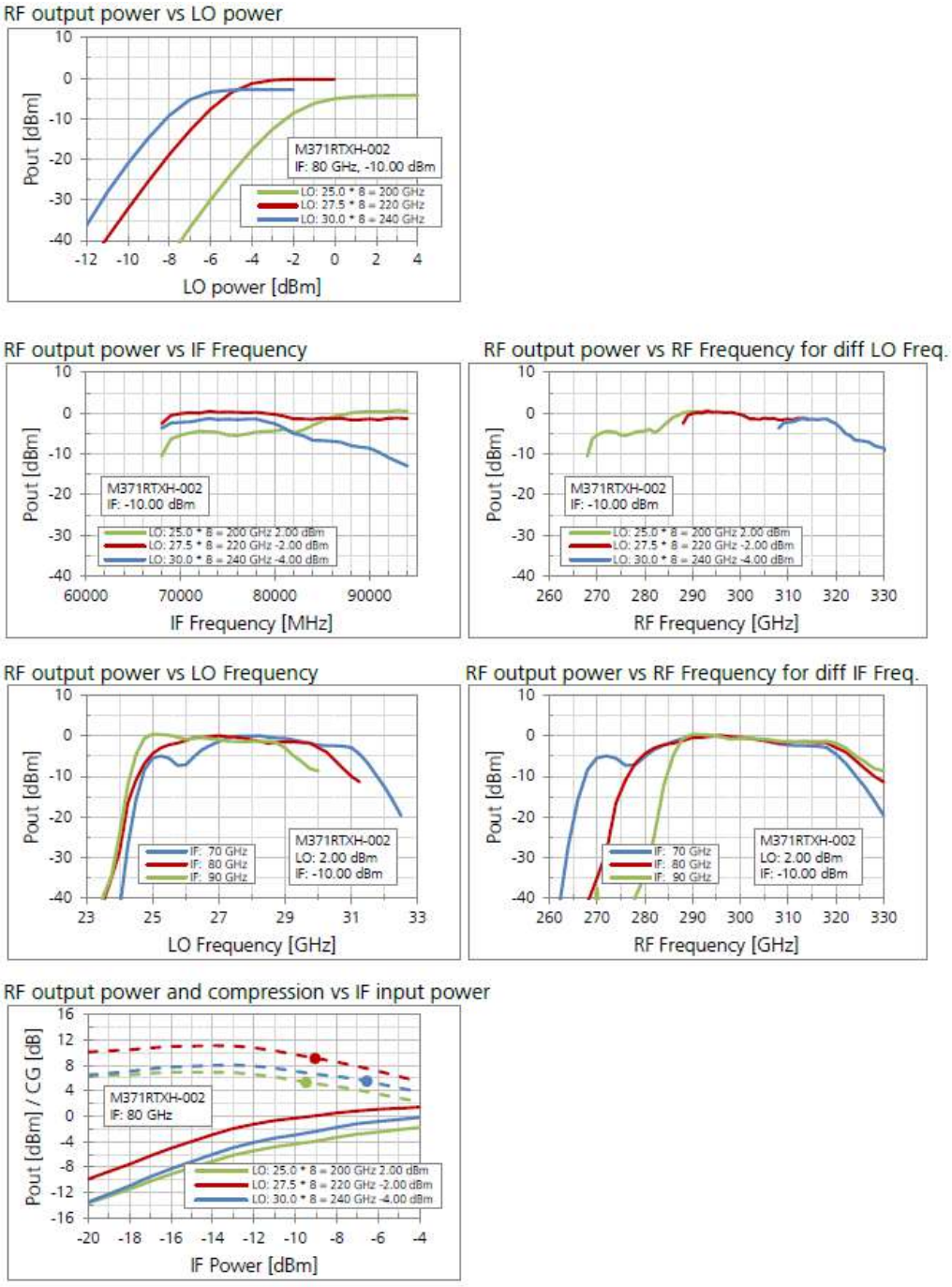

Figure 21: Measured performance of the Tx THz module

3.2 Rx-Module Characterization

Table 2: Summary of the Rx-module performance.

Port	Parameter	Min	Typ	Max
DC	DC voltage @ connector	3.5 V	3.8 V	5 V
	DC current		250 mA	275 mA @ P-LO 2 dBm
	DC connector	SMB		
LO-IN	LO-IN input power	-4 dBm	2 dBm	4 dBm
	LO-IN input frequency	25 GHz		33 GHz
	LO-IN connector	V-Connector		
RF-IN	RF-IN input power		-35 dBm	-20 dBm
	RF-IN frequency range	270 GHz		330 GHz
	RF-IN connector	H-Band waveguide (WR-3)		
IF	IF conversion gain		0 dB	
	IF frequency	60 GHz		90 GHz
	IF connector	E-Band waveguide (WR-12)		

*) all values referred to module interface

The receiver module “M371RRXH” developed and manufactured in the frame of the TIMES project was assembled using the identical approach than for the Tx-module and characterized in a calibrated waveguide environment, identically to the transmitter as well. A summary of the Tx-module performance is presented in Table 2. The measurements of the module are shown in Figure 22.

In the plot “Conversion gain vs LO power”, the conversion gain increases strongly with LO drive level for all investigated LO frequency bands. As the LO power is increased, the conversion gain rises rapidly and reaches saturation between about −6 dBm and 2 dBm LO power. In the saturated regime, peak conversion gains of roughly 10–13 dB are achieved. Higher LO frequencies around 240 GHz reach saturation earlier and exhibit slightly higher maximum conversion gain compared to lower LO frequencies around 200 GHz.

The plot “Conversion gain vs IF frequency” shows the conversion gain as a function of IF frequency from 60 GHz to 95 GHz at a fixed RF input power of −37 dBm. For LO frequencies around 220–240 GHz, the conversion gain remains relatively flat between about 9 dB and 13 dB over a wide IF band from roughly 65 GHz to 85 GHz. At lower LO frequencies, the conversion gain decreases more noticeably toward the lower end of the IF band, dropping below 0 dB near 60 GHz. Above about 85–90 GHz IF frequency, a gradual roll-off of several dBs is observed for the 240 GHz LO settings.

In “Conversion gain vs RF frequency for diff LO freq.”, the conversion gain is plotted versus RF frequency from about 260 GHz to 330 GHz for different LO frequency ranges. The receiver exhibits a broad RF bandwidth with conversion gain values typically between 8 dB and 14 dB over a central RF range of approximately 285–315 GHz. At lower RF frequencies below 270 GHz, the conversion gain drops sharply, in some cases below −20 dB, indicating the lower edge of the RF operating band. Toward higher RF frequencies above 320 GHz, the conversion gain decreases again by roughly 5–10 dB, depending on the LO frequency.

The plot “Conversion gain vs LO frequency” illustrates the dependence of conversion gain on LO frequency between approximately 23 GHz and 33 GHz for several IF frequencies ranging from 60 GHz to 90 GHz. For all IF settings, the conversion gain increases steeply as the LO frequency enters the optimal region around 27–28 GHz. Maximum conversion gain values of about 10–15 dB are obtained between roughly 26 GHz and 30 GHz LO frequency. Outside this region, particularly below 24 GHz and above 31–32 GHz, the conversion gain degrades significantly, dropping by more than 15–20 dB at the band edges.

In “Conversion gain vs RF frequency for diff IF freq.”, the RF frequency response is shown for IF frequencies of 60 GHz, 70 GHz, 80 GHz, and 90 GHz at a constant LO power of −2 dBm. Peak conversion gains close to 12–14 dB are achieved for IF frequencies of 70–90 GHz in the RF range between approximately 290 GHz and 315 GHz. For the lowest IF frequency of 60 GHz, the conversion gain is reduced, remaining mostly between 4 dB and 8 dB over the same RF band. At RF frequencies below 275 GHz and above 325 GHz, the conversion gain drops sharply for all IF settings.

The second “Conversion gain vs IF frequency” plot highlights the influence of RF input power on the IF bandwidth. For RF input powers between −37 dBm and −20 dBm, the conversion gain increases with RF power, reaching approximately 12–13 dB at low RF input levels and decreasing to around 6–8 dB at higher RF input powers. Across the IF frequency range from about 65 GHz to 90 GHz, the conversion gain remains relatively flat for a given RF power, with variations typically within ±1–2 dB.

Finally, the graph “Conversion gain vs RF power” presents the large-signal behavior of the receiver at an IF frequency of 80 GHz. At low RF input powers around −37 dBm, the conversion gain is approximately 12 dB. As the RF input power increases, the conversion gain gradually decreases due to gain compression, dropping to about 5–6 dB at RF input powers near −18 dBm. The indicated 1 dB compression point occurs at an RF input power of approximately −28 dBm, defining the upper limit of the linear operating range.

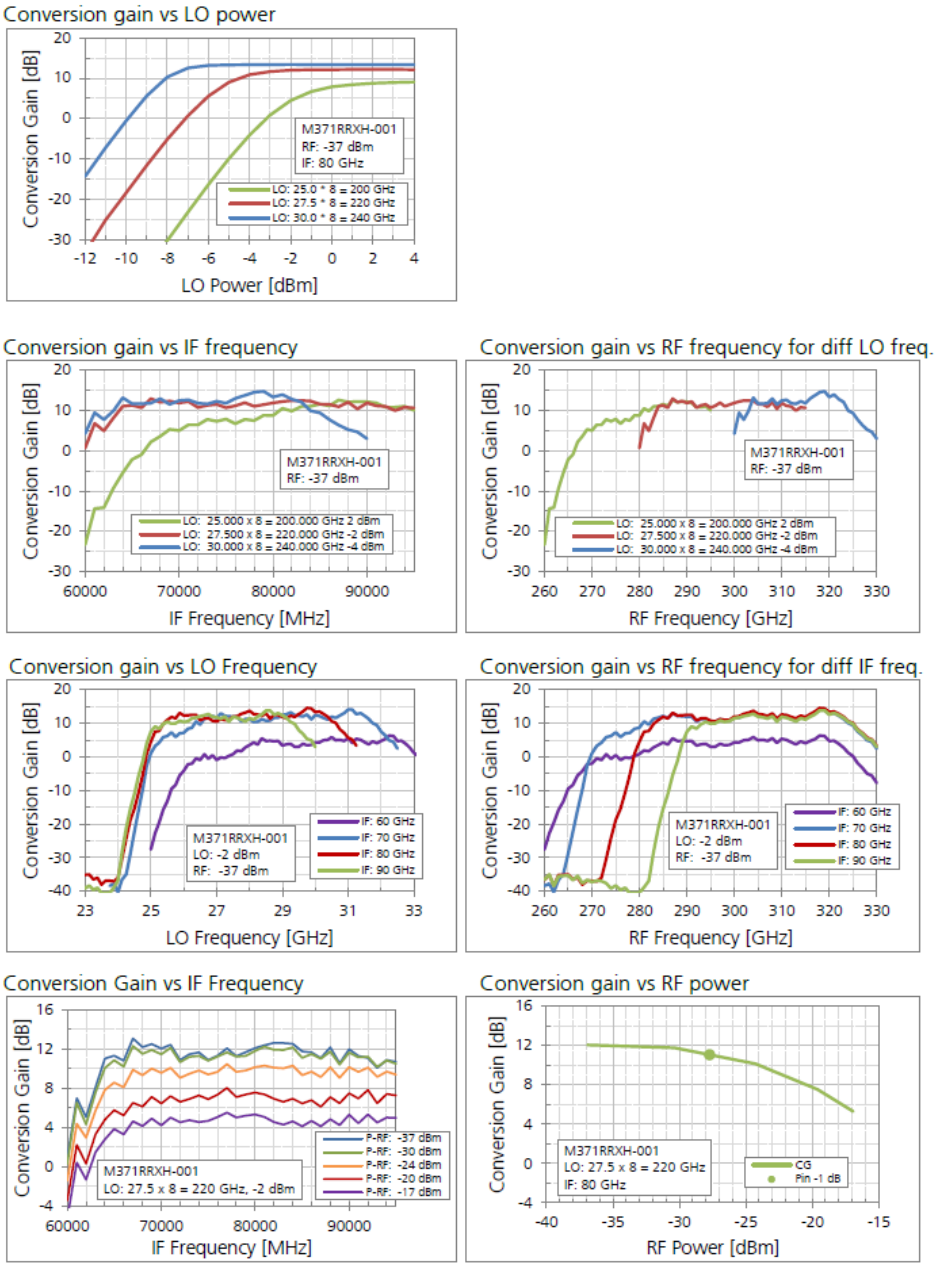

Figure 22: Measured performance of the Rx THz module

3.3 Medium Power Amplifier Characterization

This chapter presents the characterization results of the TIMES THz medium power amplifier module. The power amplifier module was assembled using the identical approach described in the Tx module implementation and the Rx module implementation chapters. All measurements presented in this chapter were performed at 3.6 V and 670 mA and are presented in Figure 23.

In the upper plot, the measured S-parameters are presented as a function of frequency from 255 GHz to 335 GHz. S_{21} exhibits a rapid increase up to values around 15 dB at 265 GHz, reaching a maximum of 20 dB in the central band between 280 GHz and 310 GHz. Beyond about 310 GHz, S_{21} gradually decreases and reaches values near 10 dB at 335 GHz. The input reflection coefficient S_{11} remains better than −10 dB over most of the band and typically lies between −15 dB and −25 dB, indicating good input matching across a wide frequency range. The output reflection coefficient S_{22} shows values around −10 dB to −15 dB over the central band, with some degradation toward the upper end of the frequency range, where S_{22} approaches −8 dB to −10 dB. Overall, the S-parameter data confirm broadband gain with acceptable input and output matching over an RF bandwidth of approximately 45 GHz.

The middle graph shows gain and RF output power as a function of RF input power for several operating frequencies between 275 GHz and 310 GHz. In the small-signal regime, for input powers below approximately −16 dBm, the gain is nearly constant and ranges from about 16 dB at 275 GHz up to around 19–20 dB at 290–300 GHz. As the input power increases, gain compression becomes visible, with a gradual reduction of gain as the amplifier approaches saturation. The corresponding RF output power increases almost linearly from 0 dBm at low input levels and reaches output power levels of approximately 7–8 dBm at input powers around −6 dBm. The indicated compression points show that the 1 dB gain compression occurs at input power levels between roughly −14 dBm and −10.5 dBm, depending on frequency, corresponding to output powers in the range of about 2–7 dBm.

The lower plot presents the gain as a function of RF output power for frequencies between 275 GHz and 315 GHz, emphasizing the saturation and compression behavior. At low output power levels below about 3 dBm, the gain remains close to its small-signal value, with peak gains of approximately 20 dB at 290–300 GHz and around 17 dB at 275 GHz. As the output power increases beyond 5 dBm, gain compression becomes more pronounced. At output power levels of approximately 8–9 dBm, the gain drops by several dBs, reaching values around 14–15 dB, depending on frequency. The highest saturation output power is observed around 290–300 GHz, where output powers close to 9 dBm are achieved before a strong gain roll-off occurs. At higher frequencies such as 315 GHz, both the maximum gain and the achievable saturated output power are reduced, consistent with the reduced small-signal S_{21} observed at the upper edge of the band.

Taken together, these measurement plots demonstrate broadband small-signal gain exceeding 15 dB, good input and output matching over a wide RF range, and saturated output power levels approaching 8–9 dBm, with well-defined compression behavior.

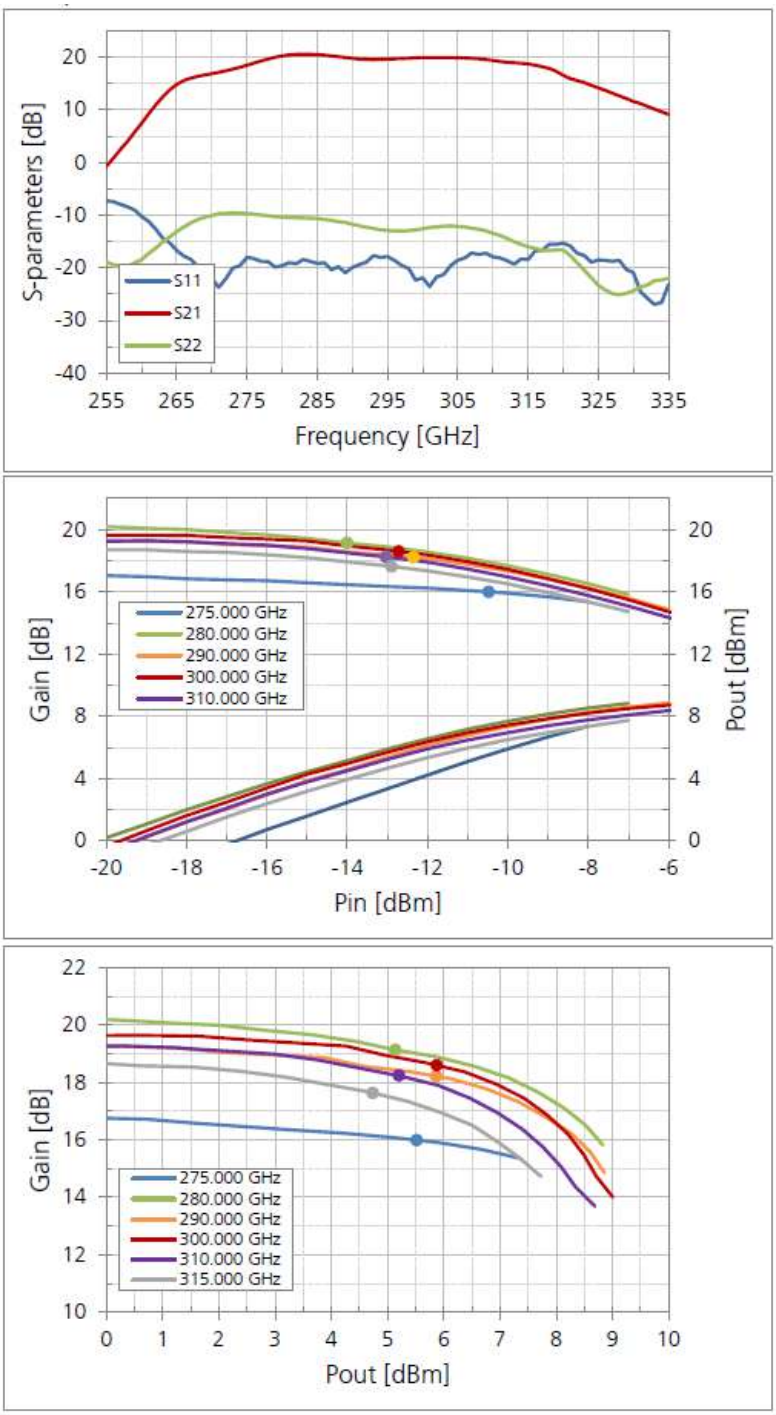

Figure 23: Measured performance of the MPA module

In addition to the module-level characterization, additional amplifier MMICs with enhanced output-power capability were evaluated. Figure 24 shows the fabricated amplifier (named "AMP126MF300") while Figure 25 and Figure 26 depict its small and large-signal measurements.

Small-signal results for AMP126MF300 indicate that from 250–335 GHz the gain (S_{21}) peaks at approximately 15 dB within 275–315 GHz and rolls off outside this band. Input match (S_{11}) remains below roughly −8 dB

across most of the span, evidencing moderate input matching. Output match (S_{22}) shows stronger frequency dependence, with portions of the band nearing -5 dB. At a fixed input drive of +1 dBm, the measured output power closely tracks S_{21}, confirming predominantly small-signal operation across the measured range.

Large-signal characterization at 300 GHz was conducted for drain voltages between 0.8 V and 1.2 V at a constant drain current density of 300 mA/mm. At 0.8 V, the small-signal gain is 15 dB and gain compression occurs at 9 dBm output power. Increasing drain voltage elevates both small-signal gain and the maximum output before compression. At 1.1–1.2 V, gain exceeds 16 dB in the linear regime, and output power approaches 13–14 dBm prior to significant compression. These results show that higher supply voltage substantially improves power handling and delays the onset of compression at the target frequency.

Although this new MPA generation delivers superior output power, the particular fabrication lot exhibited reduced yield. To ensure timely assembly of sufficient modules for demonstration, the final module integration prioritized an MPA variant with slightly lower output power but more robust yield.

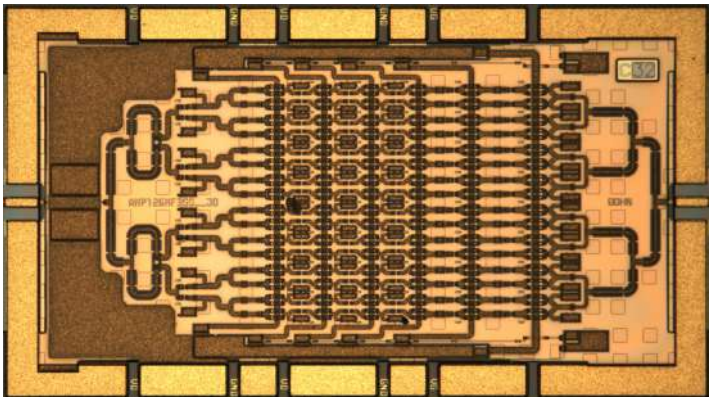

Figure 24: Chip photograph of the amplifier AMP126MF300

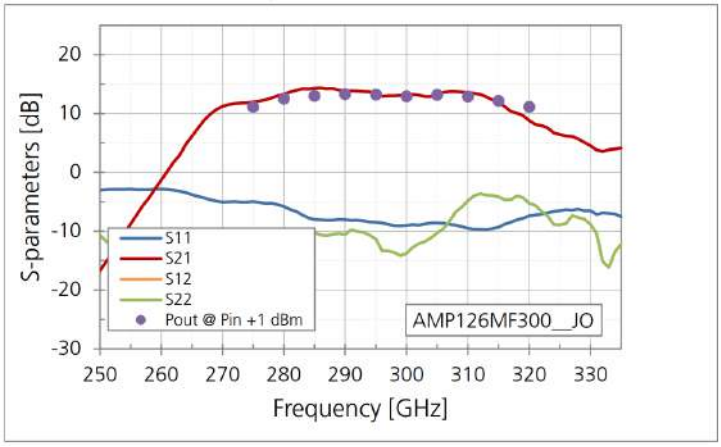

Figure 25: Small-signal two-port parameters and output power at fixed input power (1 dBm) of the medium power amplifier AMP126MF300

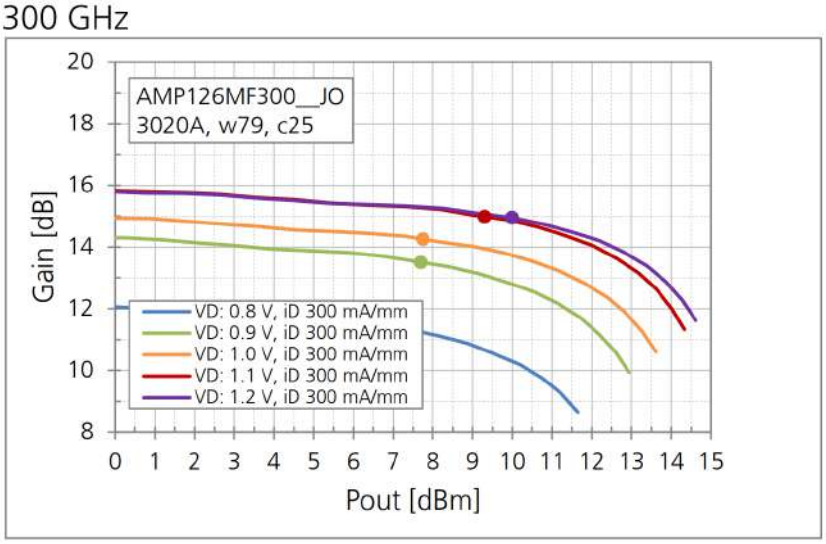

Figure 26: Large signal characterization of the medium power amplifier AMP126MF300

4 Indoor Units (IDUs) characterization

Table 3: Summary of the IDU performance.

Port	Parameter	Min	Typ	Max
DC	DC voltage @ connector	6 V	6.5 V	7 V
	DC current		3.4 A	start 3.8 A
	DC connector	Phoenix Contact, No: 1898839		
		Mate: Phoenix Contact, No: 1873058		
RX-RF-IN	RF-IN input power		-35 dBm	-20 dBm
	RF-IN frequency range	270 GHz		320 GHz
	RF-IN connector	H-Band waveguide (WR-3)		
RX-IF-OUT	IF conversion gain		10 dB	
	IF frequency	60 GHz		90 GHz
	IF connector	E-Band waveguide (WR-12)		
TX-RF-OUT	RF-OUT output power		7 dBm	
	RF-OUT frequency range	270 GHz		320 GHz
	RF-OUT connector	H-Band waveguide (WR-3)		
TX-IF-IN	IF input power		-25 dBm	-15 dBm
	IF frequency	60 GHz		90 GHz
	IF connector	E-Band waveguide (WR-12)		
USB	Communication	USB (Micro-B)		
Up/Down	Frequency-CTRL	Connector in IDU: Molex, No: 5055670451		
		Mate: Molex, No: 5055650401		
		Cable: Molex, No: 45111-0402		

*) all values referred to module interface

The measured results (see summary in Table 3) from the IDUs position the TIMES THz-Indoor-Unit as a link-ready, broadband front-end with performance that is not just adequate but repeatable and easy to integrate. The receiver characterization (see Figure 27)shows a conversion gain with reasonable droop across the entire E-band IF span (60 - 90 GHz), with traces captured at LO fundamentals of 25.2, 27.6, and 30.0 GHz (internally multiplied X8 to 201.6, 220.8, and 240.0 GHz). Under the representative small-signal condition used in the plots (RF input = −37 dBm), the Rx maintains the expected 10 dB typical conversion gain with acceptable ripple as IF frequency is swept (see “Conversion gain vs IF frequency” plot). This flatness across the IF band reduces equalization burden on the digital backend and provides a good basis to wideband modulation. Equally important, the Rx gain remains stable when the RF is swept across the WR-3 band (see “Conversion gain vs RF frequency for diff LO freq.” graph): the data confirm robust coverage from 270 to 320 GHz with only modest gain variation across LO setpoints, indicating that the waveguide transitions, mixer, and LO drive all track the band without introducing abrupt discontinuities.

The conversion gain vs RF input power measurements (see “Conversion gain vs RF power” plot) exhibit the expected monotonic reduction in power gain as the RF input level is increased, i.e., a smooth and predictable onset of compression rather than any sudden or erratic nonlinearity, which is a desired behaviour for a communication receiver.

The Rx traces taken at a controlled small-signal condition (RF = −37 dBm) establish overall a clean, comparable baseline across LO fundamentals, isolating band-dependent effects from power-dependent compression.

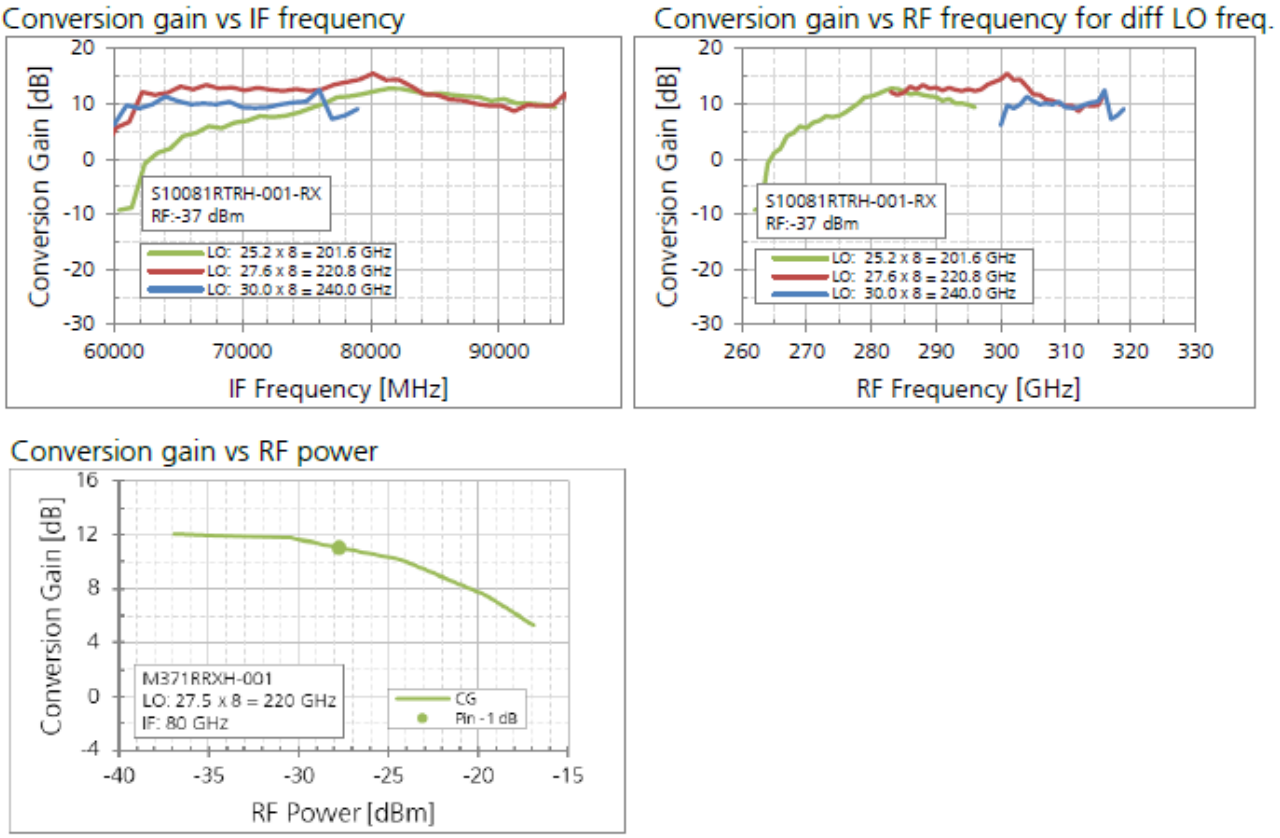

Figure 27: Measured receiver performance of the IDU

On the transmitter side, the data (see Figure 28) confirms the very good system performance. With an IF drive of −25 dBm, the measured output power versus IF frequency shows consistent behaviour across the 60–90 GHz span, with the best output near mid-E-band as expected from standard waveguide and mixer passbands (see “Conversion gain vs IF frequency” plot). The complementary RF output power vs RF frequency sweeps verify continuous RF coverage across 270–320 GHz for each of the LO fundamentals (25.2, 27.6, 30.0 GHz; X8 internally), demonstrating that tuning agility does not come at the expense of amplitude uniformity (see “RF output power vs RF Frequency for diff LO Freq.” graph). In practice, this means the unit can step across the predefined LO list (24.0–34.4 GHz fundamentals) and maintain a stable transmit envelope, simplifying calibration when changing channels or conducting swept-frequency tests.

An essential Tx result is the compression characterization at IF = 80 GHz. The plot of RF output power and compression vs IF input power (see “RF output power and compression vs IF input power” plot) shows a clear linear regime over the recommended Tx-IF drive range, followed by the expected onset of compression as

the input approaches and exceeds the upper limit. This provides an immediate, actionable operating window for clean spectral transmission. The typical Tx RF output power of 7 dBm is consistent with this behaviour when the chain is driven to its intended operating point, offering ample headroom for high-speed links and a solid basis for higher-EIRP deployments with high-gain antenna if needed.

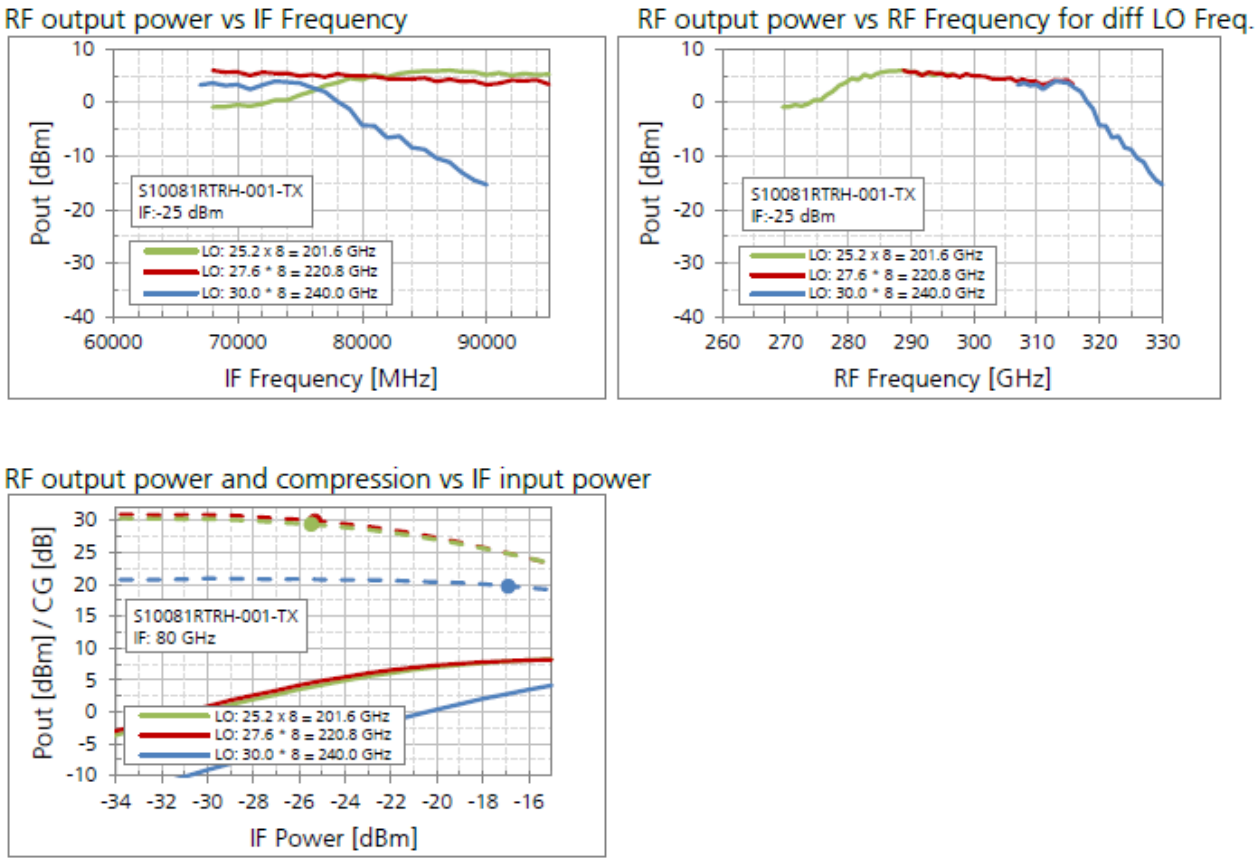

Figure 28: Measured transmitter performance of the IDU

From a practical deployment perspective, these measured characteristics translate directly into simpler link planning and more robust operation. Flat Rx gain across 60–90 GHz avoids IF "hot spots" that can require separate calibration per-band. Stable Tx power across IF and RF sweeps reduces variation in received SNR when hopping or steering. Predictable compression in both chains allows straightforward safety margins for high-order constellations. And the verified operation at multiple LO fundamentals—explicitly 25.2, 27.6, and 30.0 GHz (X8)—demonstrates that stepping through the predefined frequency list can be done without sacrificing uniformity, enabling repeatable test campaigns and rapid retuning during PoC demonstrations.

The RF band coverage of 270–320 GHz on both Rx and Tx, the IF band of 60–90 GHz with 10 dB typical Rx conversion gain, and the Tx typical 7 dBm RF saturated output power are all substantiated by the provided plots and operating conditions. Because the measurements were taken at the module interfaces, there is no ambiguity about fixture loss or external transitions; what is seen in the measurement data is what system integrators can expect on the bench. For system teams, that means tighter correlation between simulation and hardware, faster bring-up, and fewer surprises when moving from lab to field.

The IDUs measured results present a front-end that is not merely functional across the 300-GHz region, but robust, uniform, and easy to exploit. The Rx demonstrates flat, broadband conversion gain across 60–90 GHz

with dependable linearity and a clear input power window; the Tx delivers consistent output across IF and RF sweeps with a well-defined linear operating range and typical 7 dBm capability when properly driven. The LO stepping and verified operation at multiple fundamentals ensure deterministic, repeatable performance across the 270–320 GHz band. These measurements collectively “de-risk” integration: they allow a good link budgets, reasonable simple calibration, and provide the linearity and uniformity needed for high-throughput THz demonstrations—making the TIMES THz-Indoor-Unit (see Figure 29) a compelling, measurement-proven hardware for 300-GHz testbeds and trials.

Figure 29: Photograph of the Indoor Unit fully assembled

5 Conclusions

The development and characterization activities have successfully validated the architectural, mechanical, and RF design choices for the TIMES THz front ends. The integration of Tx, Rx, and MPA modules into a single compact IDU platform demonstrates the feasibility of a modular yet fully functional 300 GHz transceiver chain suitable for both laboratory demonstrations and field deployment.

From a system perspective, the combination of broadband waveguide packaging, efficient MMIC-to-waveguide transitions, and tightly integrated PLL subsystems ensures that the front ends can operate over the full 260–330 GHz RF band with stable conversion gain and predictable linearity. The Tx and Rx modules achieve their targeted IF bandwidths with reasonable gain ripple, supporting high-data-rate E-band back-end equipment. The LO generation system meets the requirements for frequency agility and spectral purity, enabling advanced functions such as beam steering and frequency hopping.

The high-gain, broadband and high output power of the MPA delivers performance in line with the targeted link budget The observed scaling of output power with drain voltage provides a clear path for further optimization, potentially enabling >10 dBm saturated output in the future.

The measured performance confirms that the implemented design and packaging strategies are effective in minimizing RF losses, maintaining thermal stability, and ensuring reproducibility at THz frequencies. The lessons learned in assembly tolerances, probe alignment, and bias integration will directly benefit future module development, with further possible additional improvements such as increase of integration level and RF performance.

The TIMES THz front ends provide a robust and high-performance platform, meeting the core technical objectives and establishing a solid foundation. The achieved results demonstrate not only the maturity of the Fraunhofer IAF mHEMT technology in the THz regime but also the viability of compact, modular transceiver architectures for emerging THz communication applications.

6 References

[1] TIMES, "D5.1 - Design and Characterization Report of the THz Circuits".

[2] TIMES, "D2.3 - Definition of scenarios and KPI for hardware"